INTERNATIONAL ATOMIC ENERGY AGENCY
UNITED NATIONS EDUCATIONAL, SCIENTIFIC AND CULTURAL ORGANIZATION
INTERNATIONAL CENTRE FOR THEORETICAL PHYSICS
I.C.T.P., P.O. BOX 586, 34100 TRIESTE, ITALY. CABLE: CENTRATOM TRIESTE

SMR.704 - 14

Workshop on Materials Science and Physics of Non-Conventional Energy Sources

(30 August - 17 September 1993)

"Thin Films for Solar Energy Utilization and for Thermal Control"

C.G. Granqvist
Department of Technology
Uppsala University
P.O. Box 534
S-751 21 Uppsala
Sweden

THIN FILMS FOR SOLAR ENERGY UTILIZATION AND FOR THERMAL CONTROL

C.G. Granqvist
Department of Technology
Uppsala University
P O Box 534, S-751 21 Uppsala, Sweden

(Summary of lectures on "Surface Coatings with Spectral and Angular-dependent Selectivity" and "Chromogenic Thin Films for Energy-Efficient Windows" given 2 and 3 September 1993 at the Workshop on Materials Science and Physics of Non-Conventional Energy Sources, ICTP, Trieste, Italy)

I. INTRODUCTION

Materials with tailor-made radiative properties are useful for harnessing the Sun's energy, for creating a new energy-efficient architecture, etc. The materials optimization must be done with consideration of the radiation that prevails naturally in our surroundings. This paper discusses this "natural" radiation, and uses its characteristic properties to devise materials for efficient solar absorption, for passive radiative cooling, and for various types of windows in energy-efficient buildings. Emphasis is put on large-area chromogenics, which enables "smart windows" to be realized. A particularly interesting possibility is to use electrochromic thin films to regulate the throughput of radiant energy so that a desirable indoor temperature and a desirable level of illumination are maintained.

Section II below introduces spectra for thermal and solar radiation, for atmospheric absorptance, and for visible and photosynthesis-active light. This information leads naturally to a series of materials - often used as thin films - for energy efficiency and solar energy conversion. We then focus on electrochromics, and Section III reports on a basic device design, a case study for the electrochromism in tungsten oxide, general considerations for the microstructure and electronic bands in electrochromic oxides, and some practical approaches to smart windows. Section IV gives a few final remarks.

II. AMBIENT RADIATION AND MATERIALS OPTIONS

A. Ambient Radiative Properties

The basic principles of materials for energy efficiency and solar energy conversion can be grasped only if one has a clear idea of the radialton that prevails in our natural surroundings.[1] This radiation is introduced in Fig. 1, where the different spectra are drawn with a common logarithmic wavelength scale.

It is convenient to start with the ideal blackbody, whose emitted spectrum - known as the Planck spectrum - is uniquely defined if the absolute temperature is known. Planck's law is a consequence of the quantum nature of radiation. Part (a) of Fig. 1 depicts Planck spectra for

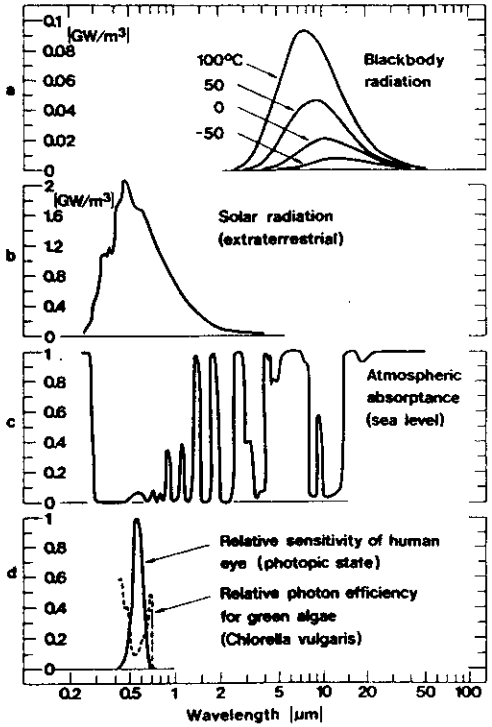

Fig. 1 Spectra for (a) blackbody radiation pertaining to four temperatures, (b) solar radiation outside the earth's atmosphere, (c) typical absorptance across the full atmospheric envelope, (d) relative sensitivity of the human eye and relative photon efficiency of green algae. (From Ref. 1).

four temperatures. The vertical scale denotes power per unit area and wavelength increment (hence the unit GW m^{-3}). The spectra are bell-shaped and confined to the $2 < \lambda < 100$ μm wavelength range. The peaks in the spectra are displaced toward shorter wavelength as the temperature goes up. At room temperature the peak lies at about 10 μm. Thermal radiation from a real material is obtained by multiplying the Planck spectrum by a numerical factor - the emittance - which is less than unity. In general, the emittance is wavelength dependent.

Figure 2(b) reproduces a solar spectrum for radiation outside the earth's atmosphere. The curve has a bell shape defined by the sun's surface temperature (~6000°C). One observes that the solar spectrum is limited to the $0.25 < \lambda < 3$ μm interval, so that there is almost no overlap with the spectra for thermal radiation. Hence one can have surfaces whose properties are entirely different with regard to thermal and solar radiation. The integrated area under the curve gives the solar constant (1353±21 W m^{-2}); this is the largest possible power density on a surface oriented perpendicular to the sun in the absence of atmospheric extinction.

The solar energy conversion systems of concern to us here are to be placed at ground level, and it is of obvious interest to consider to what extent atmospheric absorption influences solar irradiation and thermal emission. Figure 1(c) illustrates a typical absorption spectrum vertically across the full atmospheric envelope at clear weather conditions. The spectrum is found to be quite complicated with bands of high absorption - caused mainly by water vapour, carbon dioxide, and ozone - and intervening bands of high transparency. It is evident that the majority of the solar radiation can be transmitted down to ground level, and only parts of the ultraviolet ($\lambda < 0.4$ μm) and infrared ($\lambda > 0.7$ μm) tails are strongly damped. The maximum power density perpendicular to the sun is limited to about 1000 W m^{-2}. Thermal radiation from a surface exposed to the clear sky is seen to be strongly absorbed except in the $8 < \lambda < 13$μm range, where the transmittance can be large provided that the humidity is moderately low. The thermal radiation can be large in the $8 < \lambda < 13$ μm interval, and hence one concludes that a non-negligible part of the emitted energy can go straight through the atmosphere. This phenomenon constitutes the basis for radiative cooling.

Figure 1(d) illustrates two biophysical constraints of interest for applications. The solid curve shows the relative spectral sensitivity of the human eye in its light-adapted (photopic) state. The bell-shaped curve extends across the $0.4 < \lambda < 0.7$ μm interval and has its peak at 0.555 μm. It is obvious that a large part of the solar energy comes as infrared radiation. Photosynthesis in plants operates with wavelengths in approximately the same range as those for the human eye, which is of relevance for greenhouse applications. An example of the relative photon efficiency for green algae is given by the dashed curve.

B. Surfaces for Selective Absorption of Solar Energy

An energy-efficient solar collector should absorb the incident solar radiation without giving off too much thermal radiation to the ambience. In optical terms, this means that the reflectance should be low up to λ_c and high beyond λ_c, where the cut-off wavelength λ_c should be between 2 and 3 μm depending on whether the operating temperaturee is high or low.[2]

It is possible to exploit several different design principles and physical mechanisms in order to create solar-absorbing surfaces with the desired spectral selectivity.[2] Six of these are shown schematically in Fig. 2. The most straightforward one is to use a material whose *intrinsic radiative properties* are spectrally selective. Generally speaking, this approach has not been very fruitful, but work on some transition metal diborides and cobalt oxides indicates that intrinsically selective materials do exist.

Semiconductor-metal tandems can give the desired spectral selectivity by absorbing short-wavelength radiation in a semiconductor whose bandgap is ~0.6 eV (such as in Si) and having low thermal emittance as a result of the underlying metal. The useful semiconductors have too large refractive indices, which tends to yield high reflection losses. Hence it is necessary to antireflect the surfaces in the range of solar radiation.

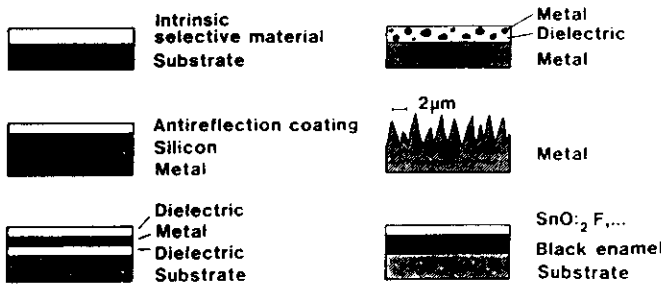

Fig. 2 Schematic designs of six different coatings and surface treatments for selective absorption of solar energy. (From Ref. 2).

Multilayer absorbers can be tailored so that they become efficient selective absorbers of solar radiation. It is comparatively easy to compute their optical performance, which facilitates optimization of the design. One interesting example is $Al_2O_3/Mo/Al_2O_3$, which was originally developed for space applications.

Metal-dielectric composite coatings consist of very fine metal particles in a dielectric host. The ensuing optical properties can be intermediate between those of the metal and of the dielectric. Effective medium theories are of great value for modelling the optical performance.[3] The metal-dielectric concept offers a high degree of flexibility, and the optimization of the solar selectivity can be made with regard to the choice of constituents, coating thickness, particle concentration, and the size, shape, and orientation of the particles. The solar absorptance can be boosted by use of suitable substrate materials and antireflection treatments. The composite coatings can be produced by a variety of techniques such as electroplating, anodization, inorganic colouration of anodized aluminium, chemical vapour deposition and codeposition of metal and insulator by evaporation and sputtering.

Textured surfaces can produce a high solar absorptance by multiple reflections against metal dendrites that are ~ 2 μm apart, while the long-wavelength emittance is rather unaffected by this texture.

The final concept considered here involves a *selectively solar-transmitting coating on a blackbody-like absorber.* The absorber can be chosen from among materials with proven long-term durability (such as black enamel), and the coating can be a heavily doped oxide semiconductor (for example SnO_2:F).

The spectral selectivity that can be achieved in a practical multilayer structure is illustrated in Fig. 3.[3,4] The shown material was produced by magnetron sputtering technology and is currently used for solar powered electricity generation in large plants operated i California. A metal-dielectric composite coating is the essential cause of the spectrally selective properties with high absorptance at $\lambda < 2$ μm and low emittance

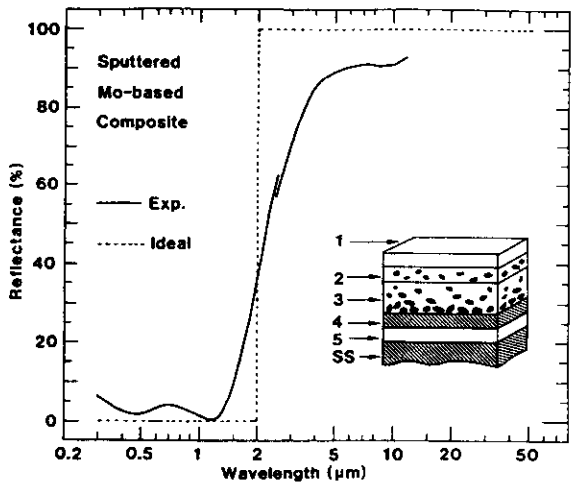

Fig. 3 Spectral reflectance measured for a molybdenum-based sputter deposited coating. Dotted lines represent an ideal reflectance profile. Inset shows the coating microstructure with five superimposed layers. They comprise, from the top: SiO_2 (1), graded Mo-SiO_2 (2), graded Mo-Al_2O_3 (3), molybdenum (4), and Al_2O_3 (5). The substrate is of stainless steel (SS). (From Refs. 2 and 4).

at $\lambda > 2$ μm. The optical performance can be understood in considerable detail from effective medium theory.

C. Materials for Passive Radiative Cooling

It was pointed out in Fig. 1 that the atmosphere can be almost transparent in the $8 < \lambda < 13$ μm range, which lies in the middle of the blackbody spectrum pertaining to normal ambient temperatures. An object with high emittance in this "atmospheric window", and oriented towards the clear sky, hence can experience a continous heat loss of the order of 100 W/m2.[5]

If one only considers radiation balance, it can be shown that temperature drops to ~50°C below the air temperature would be possible. Conduction

and convection in a practical cooling device limit the temperature drop, but temperature differences around 20°C are feasible.[5]

Radiative cooling requires two new types of materials in order to be optimized: a selective infrared radiator with high emittance at $8 < \lambda < 13$ μm and low absorptance elsewhere, and a mechanically rigid infrared-transparent convection shield. Selective infrared radiators have been developed by exploiting the radiative properties of silicon-based coatings backed by metal.[5] The Si-O and Si-N vibrational modes jointly cover the $8 < \lambda < 13$ μm range; the properties can be modeled from effective medium theory with due consideration of the various Si-centered tetrahedra constituting the oxynitride.[6] Among the other approaches to selective infrared emission we note certain polymer foils with metallic backings, gas slabs (C_2H_4, C_2H_4O, NH_3) backed by metal,[7] and some ceramic oxide layers with their Reststrahlen band at $\lambda > 13$ μm.[5] The required transparent convection shields can be constructed from corrugated high-density polyethylene.

The potential of radiative cooling is illustrated here with reference to a simple experiment in which a slab of C_2H_4 gas, confined by a low emittance surface and an infrared-transparent foil, was exposed to the sky in full daylight (direct solar radiation was blocked). Figure 4 shows the result of a cooling test.[7] At point A, a C_2H_4 flow was started, and a difference between the inlet temperature τ_{in} and the outlet temperature τ_{out} was noticed. In the experiment, τ_{in} was close to the ambient temperature τ_a. At point B, the gas flow was stopped; now the temperature difference became as large as ~ 10°C. It is easy to induce self-circulation of the radiatively cooled gas.

An interesting application of radiative cooling is in water condensation. If a surface is cooled so that its temperature is lower than the dewpoint, while the surrounding nature is above the dewpoint, there will be a preferential condensation of atmospheric humidity. As much as ~ 0.5 l of water per m^2 and per night has been recorded even under fairly arid conditions. This opens avenues towards "condensation irrigation".

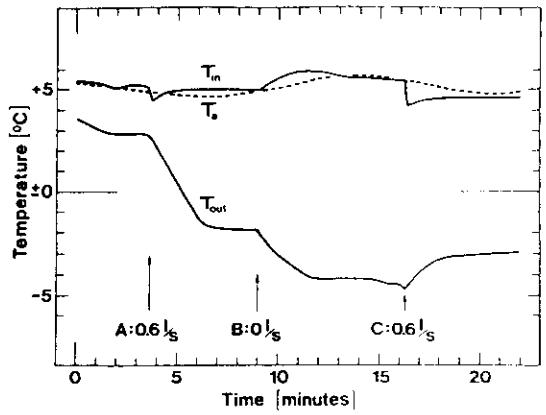

Fig. 4 Excerpt from an experiment for testing radiative cooling with a 10-cm-thick slab of C_2H_4. τ_{in} and τ_{out} denote the temperatures at the gas inlet and outlet, respectively, and τ_a is the ambient temperature. At A, B and C, the gas flow was adjusted to the shown rates. (From Refs. 5 and 7).

Another approach to radiative cooling makes use of heavily pigmented polyethylene foils having a high solar reflectance yet they are transparent in the $8 < \lambda < 13$ μm range. Such foils can produce a marginal cooling - or at least prevent heating - of whatever is covered by the foil and exposed to the clear sky. Here we have the "cooling wrapping paper".

D. Survey of Coatings for Energy Efficient Windows

Coatings can be used on windows for obtaining several different goals. Table I summarizes these goals, gives the principle solutions, and lists the different types of materials used in the coatings.[8] In a warm climate, the windows normally let in too much energy, which must be balanced by air conditioning. The situation can be alleviated if the windows have coatings that are transparent primarily for visible light, i.e. at $0.4 < \lambda < 0.7$ μm, whereas they are reflecting for near-infrared solar radiation at $0.7 < \lambda < 3$ μm. A thin metal (Me) film can combine a transmittance of

Table I. General properties of coatings for energy-efficient windows

Goal	Principle solution	Coating material*
Diminished solar heating	Reflectance at $0.7 < \lambda < 3$ μm	Me or D/Me/D
	Angular dependent transmittance	D/Me/D/Me/D Oblique columnar metal
Thermal insulation	Reflectance at $3 < \lambda < 50$ μm	D/Me/D, SnO_2:F;In_2O_3:Sn, ZnO:Al,...
Dynamic radiation control	Absorptance or reflectance in electrochromic material	Li_xWO_3, NiO_xH_y,... in multilayer design with transparent ion conductor
	Reflectance at $0.7 < \lambda < 3$ μm in thermochromic material	VO_2-based
Higher transmittance	Antireflectance at $\lambda \approx 0.55$ μm	AlO_xF_y,...

* Me is Ag, Cu, Au (or Al); D is Bi_2O_3, In_2O_3, SnO_2, TiO_2, ZnO or ZnS.

~ 50 % in the visible range with a high infrared reflectance. However such a film is too absorbing for many applications, and instead the metal film could be put between two dielectric (D) layers which, in effect, antireflect the metal. A D/Me/D coating with Me = Ag can have ~ 80 % visible transmittance.

Another way to diminish the solar inflow is to exploit angular-selective window coatings.[9,10] The underlying idea is that windows are devices for creating visual contact with the outside world along an approximately horizontal line-of-sight, whereas solar radiation normally enters from a point much higher up on the vault of heaven. It follows that one can obtain energy efficiency by having films with high transmittance horizontally and a much lower transmittance at other angles. A properly tailored D/Me/D/Me/D coating can be useful for ordinary vertical windows.

Angular selectivity can be created also for sloping windows; in this case the film can be comprised of inclined columns produced by oblique angle vacuum deposition. For the latter case, one has a higher transmittance along the columns than across them, as one expects from effective medium theory.

In a cold climate, one normally wants to combine a high solar transmittance at $0.3 < \lambda < 3$ μm with a high reflectance (i.e., a low emittance) for thermal radiation at $3 < \lambda < 50$ μm. Metal-based D/Me/D coatings can be optimized for these wavelength intervals, but it may be more cost-effective to invoke films of certain heavily doped wide-bandgap oxide semiconductors such as In_2O_3:Sn, SnO_2:F, SnO_2:Sb and ZnO:Al. When the doping level is high enough so that the Mott critical density is exceeded, the semiconductors become strongly n-doped and can be reflecting at wavelenghts longer than the plasma wavelength that can be between 1 and 3 μm depending on the doping level and the degree of crystallinity.[11,12]

The heavily doped semiconductors are amenable to quantitative theoretical analysis.[11,12] Essentially, three components are added to form the complex dielectric function, viz.

- the *contribution due to bound electrons*, accounting for bandgap widening due to the Burstein Moss effect partly balanced by electron-ion and electron-electron interaction,[13,14]
- the *contribution due to free electrons* undergoing ionized impurity scattering against Coulomb potentials screened in accordance with the Random Phase Approximation or an extension thereof, and
- *phonon contributions* that can be modeled as a series of Lorentz oscillators.

The full theory allows the optical properties to be computed. Figure 5 shows an example for the transmittance and reflectance of a 0.2-μm-thick film of In_2O_3:Sn doped so that the electron density n_e had the shown values.[11] Clearly, increasing the electron (or, equivalently, the dopant) density gives a material combining a high visible transmittance with a high

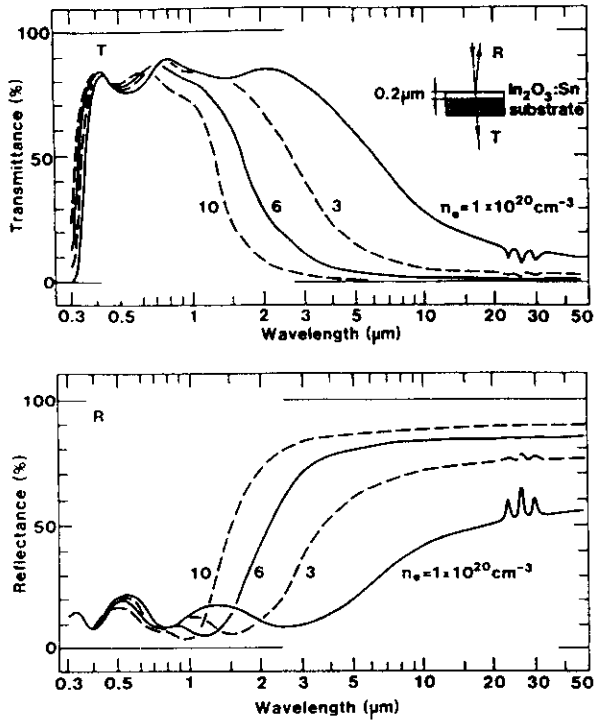

Fig. 5 Spectral normal transmittance (upper part) and reflectance (lower part) computed from a quantitative model for the optical properties of In_2O_3:Sn. The shown values of electron density (n_e) and coating thickness were used. (From Refs. 8 and 11).

thermal infrared reflectance. Properly made In_2O_3:Sn films have optical properties in excellent agreement with the theoretical model.

A dynamic control of the optical properties is possible in smart windows with chromogenic coatings. The presently most viable alternatives are electrochromic films in multilayer devices, as we discuss in the following section, and thermochromic films. Among the thermochromic films, the most important ones are based on VO_2. This material undergoes a transformation from a semiconducting and rather transparent state to a metallic and less transparent state when a temperature of ~ 68°C is exceeded. This phase change temperature can be diminished to room temperature by alloying with tungsten[15] and the transmittance can be boosted by fluorine

incorporation.[16] The ensuing material is of considerable interest for thermochromic smart windows.

III ELECTROCHROMICS AND SMART WINDOWS

A. Background

Electrochromic devices are able to change their optical properties in a reversible and persistent manner under the action of a voltage pulse. The optical modulation is related to the amount of mobile ions in an electrochromic material, which here is taken to be a metal oxide. The devices comprise several layers backed by a substrate (normally a glass plate) or layers positioned in between two substrates in a laminate configuration.[17] The substrate has a transparent conducting film and a film of the electrochromic oxide. Then follow a fast ion conductor or electrolyte, a layer serving as ion storage - which can be another electrochromic material - and a second (transparent) conductor. When a voltage is applied between the (transparent) conductors, ions are inserted into or extracted from the electrochromic film, whose optical properties thereby are changed. The design is outlined in Fig. 6. The insertion/extraction process can be represented, high schematically, by

$$MeO_y + xI^+ + xe^- \leftrightarrow I_xMeO_y, \qquad (1)$$

where Me is a metal atom, I^+ is a singly charged small ion such as H^+ or Li^+, e^- is an electron, and y depends on the particular type of oxide. For example, y is 3 for defect perovskites and 2 for rutiles.

Electrochromic devices have several important applications that presently spur the scientific and technical development. Foremost among these are smart windows capable of regulating the inflow of radiant energy in buildings so that an optimum indoor climate is maintained at a minimum demand on paid energy. Electrochromism is also exploited for anti-dazzling rear-view mirrors for automobiles, for non-emissive information displays with superior viewing properties, and for sunglasses.

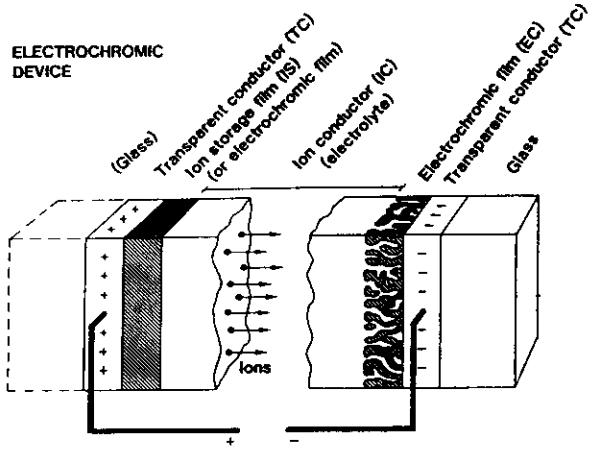

Fig. 6 Basic design of an electrochromic device, indicating transport of positive ions under the action of an electric field.

B. Electrochromism in W Oxide: A Case Study (Ref. 17)

Electrochromism was discovered in W oxide films, and this material remains still today the most promising with regard to practical applications. There are many techniques for making W oxide films. Evaporation, sputtering and a number of chemical and electrochemical methods all are applicable and are able to produce non-stoichiometric WO_3 films with a porosity of up to 50 %. Raman scattering and X-ray extinction have been used to formulate structural models[18] showing that the films are built, essentially, from clusters of corner-sharing octahedra held together by hydrogen bonds and bridging water molecules.

Electrochromism can be viewed as an electrochemical phenomenon, and W oxide films have been studied extensively in liquid electrolytes by use of the conventional techniques of electrochemistry. Coulometric titration, chronoamperometry, cyclic voltammetry, impedance spectrometry, beam deflectometry, and microbalance techniques[17] have been applied. The diffusion constants for intercalation/deintercalation of H^+ and Li^+ lie in the brackets 10^{-10} to 2.5×10^{-7} and 1.5×10^{-12} to 5×10^{-9} cm^2/s, respectively.

Among the various physical techniques used to analyze W oxide films, X-ray photoelectron spectroscopy (XPS) and electron paramagnetic resonance (EPR) have given particularly valuable information. Figure 7 shows XPS data for W-oxide-based materials in the energy range pertinent to W4f electrons. The bottom curve, for a WO_3 reference, shows two peaks corresponding to the $W4f_{7/2}$ and $W4f_{5/2}$ spin-orbit-split doublet.[19] This feature hence is due to W^{6+}. H^+ intercalation in evaporated W oxide films, reported on in the upper three curves, leads to a blurring of the doublet and the appearance of a low-energy shoulder. It is possible to get quantitative information on the amount of W atoms in different valence states by

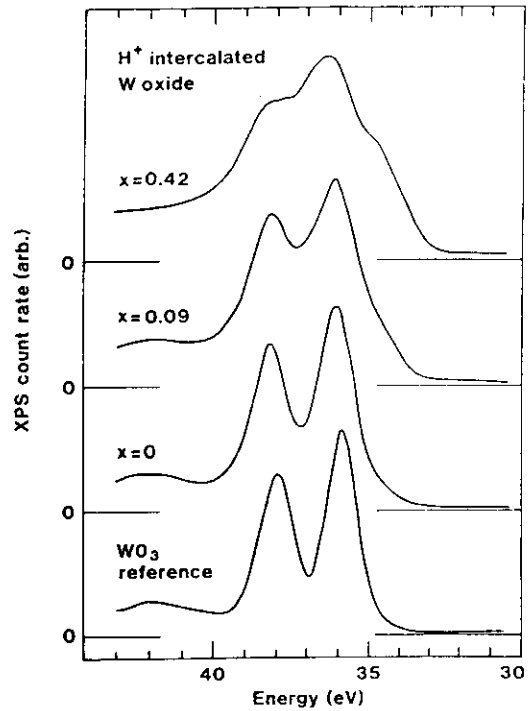

Fig. 7 XPS count rate vs. binding energy for W4f electrons with different amounts of H^+ intercalation (given as x in H_xWO_3). Bottom curve refers to a WO_3 reference sample. (From Ref. 19).

deconvoluting the XPS spectra, and for H_xWO_3 with x = 0.09 it is possible to represent the spectrum with two doublets assigned to W^{5+} and W^{6+}. At x = 0.42 there is clear evidence also for W^{4+}.

EPR is capable of providing additional information on the valence state of the W ion since W^{5+} ($5d^1$ configuration) gives a signal due to its unpaired spin whereas W^{6+} ($5d^0$ configuration) does not give any signal. Experimental data[20] showed unambiguously that a signal at g = 1.76, assigned to W^{5+}, developed upon H^+ intercalation.

Intercalation of H^+ or Li^+ leads to the development of a broad absorption band centered at $\lambda \sim 1$ μm. The intensity of this band scales accurately with the EPR signal at g = 1.92 and hence the emerging picture is that electrons, that are introduced jointly with the intercalated ions, are localized at the tungten sites where they participate in processes responsible for the absorption. From analyses of the shape of the absorption peak,[21] as well as from electrical and other data, it can be inferred that small polaron absorption is the underlying cause for the electrochromism in W oxide.

Figure 8 shows the modulation of the spectral transmittance that occurs upon intercalation to the shown charge densities in a H^+-conducting

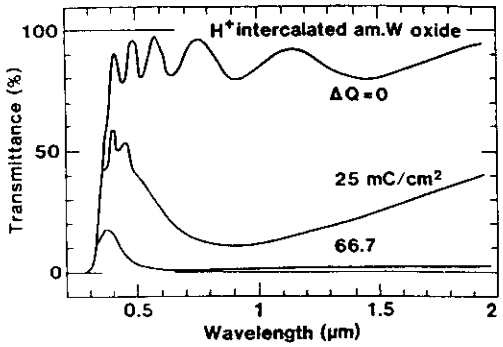

Fig. 8 Spectral transmittance for an amorphous (am.) W oxide film with H^+ intercalation to the shown charge densities. (From Ref. 22).

electrolyte.[22] It is apparent that the W-oxide-based film can change reversibly and gradually from a virtually transparent state to a state characterized by a weak transmittance of blue light.

C. Microstructure and Electronic Bands: A Unified Approach (Ref. 23)

The electrochromic oxides can be divided into three main groups with regard to their bulk crystalline structures: perovskite-like, rutile-like, and layer and block structures. They are discussed in this order below, and the ubiquity of the octahedral MeO_6 building blocks is emphasized. Reference 24 may serve as a standard source for much of the structural information. Along with the discussion of structure, we point at characteristic features of the electrochromism.

The *perovskite structure*, with a general composition $CMeO_3$, is illustrated in Fig. 9. As drawn, the Me ions occupy the corners of a primitive unit cell and O ions bisect the unit cell edges. The central atom, denoted C, is neglected at the moment since it is absent in the electrochromic oxides of most interest. The corresponding (defect) perovskite MeO_3 configuration is often referred to as the rhenium oxide structure. It can be visualized

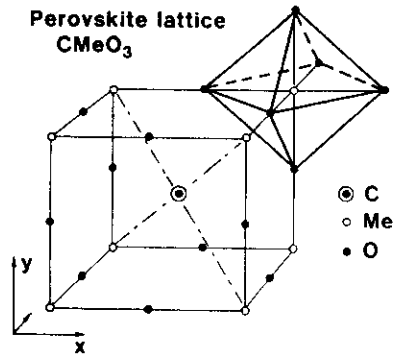

Fig. 9 Unit cell for the perovskite lattice. Octahedral symmetries are emphasized.

as an infinite array of corner-sharing octahedra each with a metal ion surrounded by six equidistant oxygen ions. In between these octahedra there are extended tunnels that can serve as conduits and intercalation sites for small ions.

Tungsten oxide, WO_3, has a crystal structure of perovskite-type, but some atomic displacements and rotations of WO_6 octahedra normally occur so that different symmetries are found. W oxide also has a tendency to form substoichiometric (Magnéli) phases with edge-sharing octahedra and extended tunnels with large pentagonal or hexagonal cross-sections. As discussed above, disordered W oxide films transform from an optically transparent to an absorbing state under ion insertion. This is referred to, in electrochemical terms, as cathodic colouration. The opposite case, with absorption associated with ion extraction, is called anodic colouration.

Molybdenum oxide, MoO_3, is another cathodic electrochromic material. Bulk crystals at room temperature have a structure consisting of corner-sharing chains of MoO_6 octahedra that share edges with two similar chains; these layers are stacked and are held together by weak van der Waal's forces. This unique structure is referred to as the α-phase. There is also a β-phase, that can be viewed as a metastable analogue of WO_3, which is of perovskite-type. Available data on thin films of Mo oxide[25] strongly indicate that the structure is built from corner-sharing MoO_6 octahedra in much the same way as for electrochromic W oxide.

The *rutile structure*, or at least a rutile-like configuration, is present for a whole series of materials exhibiting cathodic or anodic electrochromism. The ideal structure can be thought of as built from almost octahedral MeO_6 units forming infinite edge-shared chains. These chains are arranged so that they form an equal number of ideal vacant tunnels.

Titanium oxide, TiO_2, can have different crystal structures, viz. rutile, anatase and brookite. The anatase phase, which so far has attracted most interest in the context of electrochromism, consists of infinite planar double chains of TiO_6 octahedra; these chains are connected by corner-sharing. Empty sites also form double chains, or zig-zag tunnels. Cathodic electrochromism with a large degree of optical modulation was observed in some work.

Manganese oxide, MnO_2, has very complex crystal chemistry. However, most structures are built from edge-shared MnO_6 octahedra that share corner with other chains. Electrochromism was discovered recently, and ion insertion was found to lower the absorption.

Vanadium dioxide, VO_2, is of rutile-type (tetragonal) above 68°C and is monoclinic - albeit with very slight atomic displacements from the ideal rutile structure - below this temperature. Vanadium dioxide films are electrochromic and show a decrease of the absorptance under ion insertion irrespective of the temperature being below or above 68°C.

Ruthenium oxide, RuO_2, has rutile structure. Ions can be inserted and extracted, but the material remains absorbing no matter the ionic content.

Iridium oxide, IrO_2, is another rutile material. It is electrochromic and - in contrast with the electrochromic oxides discussed so far - is clearly anodic and can go from an absorbing to a fully transparent state under insertion of one ion per formula unit.

Rhodium oxide, RhO_2, shows many similarities with iridium oxide, and ion insertion is able to lower the absorption significantly.

The *layer and block structures* form a somewhat undefined group of electrochromic materials with, generally speaking, not so well explored structural properties. Hydrous Ni oxide shows pronounced anodic electrochromism and goes from an absorbing to a transparent state under proton insertion. The material is thought to contain layers of NiO_6 octahedra sharing edges, and the protonated material is probably akin to brucite, $Ni(OH)_2$.

Vanadium pentoxide, V_2O_5, can be described as consisting of distorted VO_6 octahedra or, alternatively and more properly, as consisting of square pyramidal VO_5 units. The latter representation highlights the layered structure. V pentoxide films are unique in their capacity for multi-colour electrochromism.

Niobium oxide, Nb_2O_5, has complex crystal chemistry. Various phases can be thought of as built from blocks (or columns) of NbO_6 octahedra

arranged as in a defect perovskite; a structure derived from corner-sharing rutile blocks is also known. Niobium oxide is electrochromic and goes from a transparent to an absorbing state upon ion insertion. Tantalum oxide has several similarities to niobium oxide.

Among the cobalt-oxide-related materials, both $HCoO_2$ and $LiCoO_2$ are of interest. The latter material can be represented as a layered rock-salt with alternate planes of cobalt and lithium atoms. Both of these species are surrounded by six oxygen atoms in octahedral coordination; the CoO_6 octahedra are compressed and the LiO_6 octahedra are elongated. $HCoO_2$ has a similar, though not identical, crystal structure. Absorption develops upon extraction of protons or lithium ions.

It follows from the discussion above that bulk crystals of, apparently, almost all of the well known electrochromic oxides are built from highly regular arrangements of edge-sharing and corner-sharing MeO_6 octahedra. Electrochromic thin films of these materials rarely exhibit long-range order, though. The local microstructure of the pertinent thin films has been studied in detail only for W oxide, and as pointed out above, the octahedral building blocks prevail also in "amorphous" thin films. We believe that this result is of general validity for the electrochromic oxides.

The structural similarities of the electrochromic materials makes it meaningful to discuss their optical properties from a canonical band-structure appropriate to the octahedral coordination. These highly simplified bandstructures, originally due to Goodenough[26] and presented in a particularly accessible way by Honig,[27] allow us to understand why certain perovskite-type and rutile-type electrochromic oxides become absorbing under ion insertion, others become transparent under ion insertion, and still others show at least some absorptance irrespective of their ionic content. Probably the layer and block structures can be handled in a similar way.

The *perovskite structure* was illustrated in Fig. 9. A corresponding energy level diagram for the defect perovskite - i.e. the rhenium oxide structure here denoted MeO_3 - is illustrated in Fig. 10a. The atomic *s*, *p* and *d* levels of Me are indicated, as well as the *2s* and *2p* levels of O. For WO_3 and ReO_3, the pertinent levels are *6s*, *6p* and *5d*. Each Me ion is octahedrally

surrounded by six oxygen ions, and each oxygen is linearly flanked by two Me ions. As a consequence of this arrangement, the *d* level is split up into e_g and t_{2g} levels as shown in the left-hand part of Fig. 10a. The splitting arises because the e_g orbitals point directly at the electronegative O whereas the t_{2g} orbitals point away from the nearest neighbours into empty space and are hence lower in energy. Similarly, the *O2p* orbitals are split as indicated in the right-hand part of Fig. 10a; the $2p_\sigma$ orbitals point directly at the nearest electropositive Me ions whereas the $2p_\pi$ orbitals point into empty space. In the perovskite lattice, the incipient molecular energy levels broaden into bands, whose relative widths and repulsion can be inferred from general arguments.[27]

The number of states available for electron occupancy is fixed for each band. For example, counted per MeO_3 formula unit, the t_{2g} band has a capacity for six electrons (allowing for spin degeneracy), and the p_π band has a capacity for twelve electrons (allowing for spin and electron degeneracy). The pertinent electron capacities are indicated by the numbers in the various bands in Fig. 10a. WO_3 and the iso-structural β-MoO_3 have 24 electrons in the shown bands, so that the Fermi energy lies in the gap between the t_{2g} and p_π bands. The bandgap is wide enough to render the material transparent. ReO_3, on the other hand, has 25 electrons so that the lower part of the t_{2g} band is occupied and the material should be non-transparent.

When ions and electrons are inserted according to reaction (1), the Fermi level is moved upwards in the presumed rigid-band scheme. In the case of WO_3 and β-MoO_3, the excess electrons must enter the t_{2g} band and the material, in principle, transforms from a transparent to an absorbing or from a transparent to a reflecting state depending on whether the electrons occupy localized or extended states. When the ions and the accompanying electrons are extracted, the material returns to its original transparent state. In ReO_3, the Fermi energy also moves upwards upon ion insertion, but it remains well within the t_{2g} band irrespective of the content of mobile ions. Consequently the optical properties are not expected to be changed qualitatively. Clearly, the discussion above explains why tungsten oxide and molybdenum oxide are cathodic electrochromic materials.

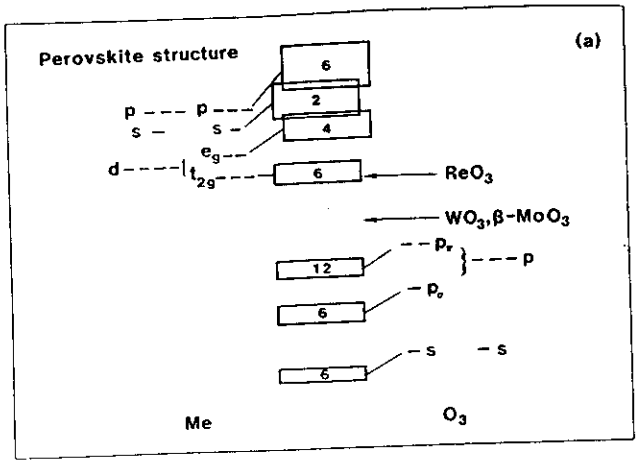

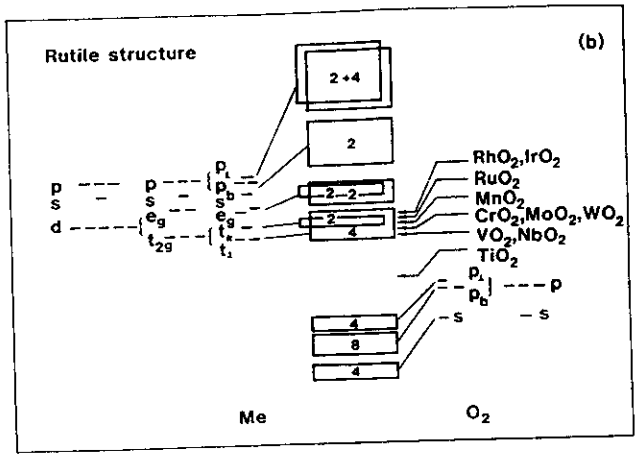

Fig. 10 Schematic bandstructures for the MeO_3 defect perovskite structure (a) and the MeO_2 rutile structure (b). The incipient atomic and molecular levels are shown, using standard notation. The numbers in the different bands denote electron capacities. Arrows indicate Fermi energies for three materials. (From Ref. 27).

Rutile and rutile-like structures are found among many MeO_2 oxides as pointed out above. Several of these are electrochromic - either cathodic or anodic - and may or may not attain a transparent state. The electrochromism can be understood from the basic bandstructure in Fig. 10b. It deviates from its counterpart for the perovskites because the MeO_6 building blocks are distorted and edge-sharing. We start from the atomic *s*, *p* and *d* levels for the Me ion and the *2s* and *2p* levels for the oxygen ions. Every Me ion is almost octahedrally surrounded by oxygen ions, and every oxygen ion is roughly trigonally surrounded by Me ions. Hence the *d* levels are first split into e_g and t_{2g} levels, and the oxygen *p* levels are split into levels with orbitals p_b in the basal plane of the triangular array (wherein the oxygen ion is surrounded by three Me ions) and with orbitals $p_\perp$ perpendicular to that array. A further splitting occurs because the ideal octahedral symmetry is absent, and the ensuing Me levels - whose origin we refrain from discussing here - are designated $t_{//}$, $t_\perp$, p_b and $p_\perp$. In addition, the degeneracy of the e_g level is lifted. When the ions are arranged in the rutile lattice, one expects overlap among the $t_{//}$ and $t_\perp$ bands as well as among the two e_g bands. Hence the final schematic bandstructure, in fact, is quite similar to that of the perovskites. Electron band capacities can be deduced as for the perovskites.

The arrows in the left-hand part of Fig. 10b indicate the Fermi levels for several rutile-like oxides. For TiO_2, the Fermi level lies in the gap between the $Ti3t_{2g}$ and the $O2p_\perp$ bands, and ion insertion is expected to lead to a transformation from a transparent to an absorbing state in much the same way as for WO_3 and β-MoO_3. This is consistent with experimental results on titanium oxide films. For VO_2, MnO_2 and RuO_2, the initial absorbing state can not be eliminated by ion insertion. Again this is as expected from the bandstructure. RhO_2 and IrO_2 are especially interesting, since their Fermi levels lie close to the gap between the t_{2g} and e_g bands. Indeed, if ions are inserted up to about one formula unit in an iridium oxide film it is transformed from an absorbing to a transparent state.[28] In the bandstructure picture, the transparency is associated with the bandgap referred to above. Rhodium oxide films are similar to iridium oxide films, but their optical properties have not been studied in great detail.

Figure 10b also lists a number of rutile-type oxides other than those mentioned above, specifically NbO_2, CrO_2, MoO_2 and WO_2. Whereas these

materials undoubtedly can be prepared as thin films, the fabrication is fairly awkward since the rutiles are not the highest oxides.

D. Towards the Electrochromic Smart Window (Refs. 17, 29)

Practical electrochromic devices have an electrolyte at their center as seen in Fig. 6. Liquid electrolytes, that are commonly used in laboratory studies, are not of interest for practical window applications. Also many of the standard members of the solid state ionics zoo (β-aluminas, Nasicons, etc.) are not easily used since it is difficult to make thin films of them. Hydrated oxide films are of relevance, and devices with a Ta_2O_5:H_2O film in between layers of cathodic electochromic W oxide and anodic electrochromic Ni oxide are currently exploited for rear-view mirrors in automobiles. Whereas this approach undoubtedly is suitable for small devices, one may question its usefulness in large smart windows to be used in energy-efficient architecture. One problem is that occasional defects and "pin holes" in the oxide electrolyte may destroy the entire device. It appears that polymer electrolytes are more promising for smart windows.

Extensive work has been carried out with proton conducting polymers such as polysulfonic acids. These polymers tend to corrode W oxide films, though, and therefore the interest has shifted more towards Li^+ conducting polymers. Initial work was reported for devices with polyethylene oxide (PEO) incorporating $LiClO_4$.[30] These "windows" exhibit thermoelectrochromism but operation at room temperature requires more conducting electrolytes. One interesting possibility is PEO-$LiN(SO_2CF_3)_2$, which was used in some recent studies.[31] Devices with amorphous W oxide and ion storage layers of V_2O_5 showed transmittance modulation between ~41 and ~13 % at λ = 0.633 μm with a time constant of ~10 s for colouration and ~2 s for bleaching. Device operation at room temperature is also possible with multilayer structures based on W oxide, V_2O_5, and an intervening electrolyte of poly propylene glycol (PPG) and poly methyl methacrylate (PMMA). Figure 11 illustrates the latter design and shows spectral transmittance in coloured and bleached states. At λ = 0.633 μm, for example, the transmittance can be modulated between as much as ~72 and ~20 %. Some results are available also with lithiated Ni oxide used as ion storage layer.

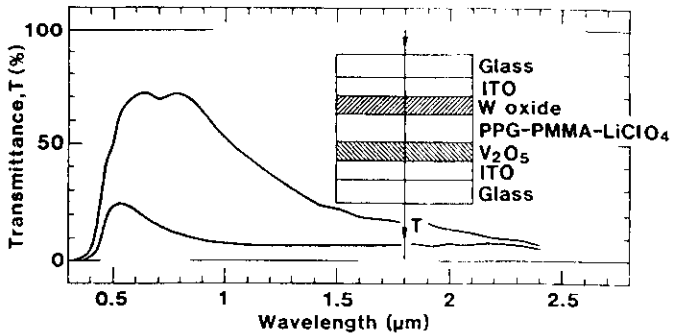

Fig. 11 Spectral transmittance in coloured and bleached states for an electrochromic device with a Li^+-conducting electrolyte. The design is sketched in the inset. (From Ref. 32).

IV CONCLUDING REMARKS

A large number of novel materials can be used for solar energy applications and for creating energy efficiency in many different contexts. Some of these materials are now reaching maturation, such as selectively solar-absorbing films of metal-insulator composites and transparen infrared-reflecting films for architectural windows. Other materials still have a way to go before they can reach commercialization; smart windows based on electrochromism and thermochromism belong to this class. Radiative cooling, and condensation irrigation based on this principle, offer intriguing possibilities in innovative technology.

Large-area chromogenics, electrochromism, and smart windows are likely to have important appplications in benign technology. Electrochromism has been known for some 25 years but has so far eluded a fundamental understanding. This paper summarized some recent advances in our understanding of the basic microstructures of the relevant oxides and of their ensuing electronic bands.

REFERENCES

1. C.G. Granqvist, editor, Materials Science for Solar Energy Conversion Systems (Pergamon, Oxford, 1991).
2. G.A. Niklasson and C.G. Granqvist, in Ref. 1, p. 70; J. Appl. Phys. 55, 3382 (1984).
3. G.A. Niklasson, in Ref. 1, p. 7.
4. M. Lanxner nad Z. Elgat, Proc. Soc. Photo-Opt. Instrum. Engr. 1272, 240 (1990).
5. C.G. Granqvist and T.S. Eriksson, in Ref. 1, p. 168.
6. T.S. Eriksson and C.G. Granqvist, J. Appl. Phys. 60, 2081 (1986).
7. E.M. Lushiku and C.G. Granqvist, Appl. Opt. 23, 1835 (1984).
8. C.G. Granqvist, in Ref. 1, p. 106.
9. G. Mbise, G.B. Smith, G.A. Niklasson and C.G. Granqvist, Appl. Phys. Lett. 54, 987 (1989).
10 G.B. Smith, M.W. Ng, R.J. Ditchburn, P.J. Martin and R.P. Netterfield, Solar Energy Mater. Solar Cells 25, 149 (1992).
11. I. Hamberg and C.G. Granqvist, J. Appl. Phys. 60, R123 (1986).
12. Z.-C. Jin, I. Hamberg and C.G. Granqvist, J. Appl. Phys. 64, 5117 (1988).
13. I. Hamberg, C.G. Granqvist, K.-F. Berggren, B.E. Sernelius and L. Engström, Phys. Rev. B 30, 3240 (1984).
14. B.E. Sernelius, K.-F. Berggren, Z.-C. Jin, I. Hamberg and C.G. Granqvist, Phys. Rev. B 37, 10 244 (1988).
15. A. Sobhan and C.G. Granqvist, to be published.
16. K.A. Khan and C.G. Granqvist, Appl. Phys. Lett. 55, 4 (1989).
17. C.G. Granqvist, in Physics of Thin Films, edited by M. Francombe and J. Vossen (Academic, San Diego, 1993), Vol. 17, p. 301.
18. T. Nanba and I. Yasui, J. Solid State Chem. 83, 304 (1989).
19. A. Temmink, O. Anderson, K. Bange, H. Hantsche and X. Yu, Thin Solid Films 192, 211 (1990).
20. P. Gérard, A. Deneuville and R. Courths, Thin Solid Films 71, 221 (1980).
21. O.F. Schirmer, V. Wittwer, G. Baur and G. Brandt, J. Electrochem. Soc. 124, 749 (1977).
22. K. Miyake, H. Kaneko, M. Sano and N. Suedomi, J. Appl. Phys. 55, 2747 (1984).

23. C.G. Granqvist, J. Mater. Sci. Engr., to be published; Appl. Phys. A, to be published.
24. B.G. Hyde and S. Andersson, Inorganic Crystal Structures (Wiley, New York, 1989).
25. P.F. Carcia and E.M. McCarron III, Thin Solid Films 155, 53 (1987).
26. J.B. Goodenough, in Progress in Solid State Chemistry, edited by H. Reiss (Pergamon, Oxford, 1971), Vol. 5, p. 145.
27. J.M. Honig, in Electrodes of Conductive Metallic Oxides, Part A, edited by S. Trasatti (Elsevier, Amsterdam, 1980), p. 1.
28. J.D.E. McIntyre, W.F. Peck, Jr. and S. Nakahara, J. Electrochem. Soc. 127, 1264 (1980).
29. C.G. Granqvist, Solid State Ionics 53-56, 479 (1992).
30. S. Pantaloni, S. Passerini and B. Scrosati, J. Electrochem. Soc. 134, 753 (1987).
31. P. Baudry, M.A. Aegerter, D. Deroo and B. Valla, J. Electrochem. Soc. 138, 460 (1991).
32 A.M. Andersson, C.G. Granqvist and J.R. Stevens, Appl. Opt. 28, 3295 (1989).